Structural consequences of the interaction of RbgA with a 50S ribosomal subunit assembly intermediate

Amal Seffouh[1], Nikhil Jain[2,3], Dushyant Jahagirdar[1], Kaustuv Basu[1], Aida Razi[1], Xiaodan Ni[4], Alba Guarné[5], Robert A. Britton[2,3] and Joaquin Ortega[1,*]

[1]Department of Anatomy and Cell Biology, McGill University, Montreal, Quebec H3A 0C7, Canada, [2]Department of Molecular Virology and Microbiology, Baylor College of Medicine, Houston, TX 77030, USA, [3]Center for Metagenomics and Microbiome Research, Baylor College of Medicine, Houston, TX 77030, USA, [4]Department of Biochemistry and Biomedical Sciences, McMaster University, Hamilton, Ontario L8S 4K1, Canada and [5]Department of Biochemistry, McGill University, Montreal, Quebec H3G 0B1, Canada

ABSTRACT

Bacteria harbor a number GTPases that function in the assembly of the ribosome and are essential for growth. RbgA is one of these GTPases and is required for the assembly of the 50S subunit in most bacteria. Homologs of this protein are also implicated in the assembly of the large subunit of the mitochondrial and eukaryotic ribosome. We present here the cryo-electron microscopy structure of RbgA bound to a *Bacillus subtilis* 50S subunit assembly intermediate (45S$_{RbgA}$ particle) that accumulates in cells upon RbgA depletion. Binding of RbgA at the P site of the immature particle stabilizes functionally important rRNA helices in the A and P-sites, prior to the completion of the maturation process of the subunit. The structure also reveals the location of the highly conserved N-terminal end of RbgA containing the catalytic residue Histidine 9. The derived model supports a mechanism of GTP hydrolysis, and it shows that upon interaction of RbgA with the 45S$_{RbgA}$ particle, Histidine 9 positions itself near the nucleotide potentially acting as the catalytic residue with minimal rearrangements. This structure represents the first visualization of the conformational changes induced by an assembly factor in a bacterial subunit intermediate.

INTRODUCTION

Significant progress in the identification of ribosome assembly factors has occurred in the past 15 years. One class of factors that is highly conserved, from bacteria to humans, are the Ribosome Associated-GTPases (RA-GTPases). These proteins have been implicated in the assembly of both the small and large bacterial ribosomal subunits and also participate in cytoplasmic, mitochondrial, and chloroplast ribosome assembly (1–3). Therefore, it is clear that this class of proteins emerged early in evolution to aid in the assembly of complex protein:RNA structures and a clear picture of how they work is critical for our understanding of the general process of ribosome biogenesis. In bacteria, several RA-GTPases including RbgA (also known as YlqF), YsxC, YphC and ObgE have been implicated in the assembly of the 50S (1).

RbgA is an essential factor for 50S subunit assembly in *Bacillus subtilis* (4–6). This protein has several homologs that have been directly shown to participate in cytoplasmic and mitochondrial ribosome assembly in yeast. The most closely related protein is Mtg1, which is similar in size and domain structure to RbgA. Importantly, Δ*mtg1* cells have a mitochondrial large ribosome subunit assembly defect that results in respiration deficiency (7). RbgA has more distant relationships with three key GTPases essential for the assembly of the yeast 60S ribosomal subunit, Nog2, Nug1 and Lsg1 (8–10).

RbgA shares conserved features with traditional GTPases represented by the Ras GTPase. One of them is to have a GTPase domain containing the G1–G2 (switch I)-G3 (switch II)-G4 motifs that coordinate the binding of the guanidine nucleotide. An important difference in RbgA is that it has a circularly permuted GTP binding domain (cpGTPase), in which the G4 region is found N-terminal of the G1–G3 region (11). Canonical members of the Ras superfamily of GTPases also contain a conserved glutamine located one amino acid C-terminal to the G3 motif that plays a vital role in GTP hydrolysis. Instead, in RbgA and several other RA-GTPases, the canonical catalytic glutamine is substituted by a hydrophobic amino acid. Thus, it was predicted that, unlike canonical GTPases, the catalytic residue in RbgA is provided by a region other than the switch II (1,12). RbgA has a slow intrinsic GTPase activity and maximum activity is typically achieved in the pres-

ence of mature 50S subunits (13–15). In addition to the N-terminal cpGTPase domain, RbgA also contains a C-terminal helical domain comprising four α-helices and a 3_{10}-helix that form a bundle.

Cells depleted of RbgA exhibit a slow growth phenotype and an abnormal ribosome profile with dramatically reduced levels of 70S ribosomes and complete lack of free 50S subunits. Instead, they accumulate a large subunit assembly intermediate migrating as a 45S particle ($45S_{RbgA}$) in the sucrose gradient (4,5). These particles show disordered functional centers and are severely depleted of tertiary binding ribosomal proteins (r-proteins) including uL16, bL27, bL28, bL33 and bL36 (16,17). However, they are still capable of maturing into a complete 50S particle (17).

Crystal structures of free RbgA from *Thermotoga maritima* (11), *Staphylococcus aureus* (18) and *B. subtills* are available. However, structures of RbgA in complex with RNA or $45S_{RbgA}$ assembly intermediates are still not available. Here, we obtained the cryo-electron microscopy (cryo-EM) structure of the $45S_{RbgA}$ particles alone and in complex with RbgA. We found that RbgA binds to the P-site and stabilizes important rRNA helices in the A and P-sites of the immature subunit. The structure unveils how helix H92 of the 23S rRNA plays a key role in stabilizing His9 in the highly conserved N-terminal end of RbgA and allowed us to propose a model for the mechanism of GTP hydrolysis in this protein that suggest how the ribosomal particle may stimulate RbgA's GTPase activity. Previous structural studies have described interactions of assembly factors with mature ribosomal subunits (19–23). Our cryo-EM structure represents the first visualization of the conformational changes induced by a bacterial assembly factor in a ribosomal subunit intermediate.

MATERIALS AND METHODS

Construction of cell strains

The mature 50S subunits and $45S_{RbgA}$ particles were purified from the initiation factor 2 (IF2)-depleted (RB419) and RbgA-depleted (RB301) *B. subtilis* strains, respectively. In these strains, genes *infB* (encoding for Initiation Factor 2) and *ylqF* (encoding RbgA) are place under the control of an isopropyl-β-D-thiogalactopyranoside (IPTG) inducible P_{spank} promotor. Construction of these strains was previously described (5).

Protein expression and purification

RbgA was overexpressed as a C-terminal His$_6$-tag protein by transforming *Escherichia coli* BL21 (DE3) cells with the pET21b-*ylqF* plasmid (5). The transformed cells were grown at 37°C in LB medium containing 100 μg/ml ampicillin to OD$_{600}$ = 0.5 and then induced by the addition of 1 mM IPTG. Cells were harvested by centrifugation after 3 h of induction and washed with 30 ml of PBS 1× buffer before resuspending it in binding buffer (20 mM Na$_2$HPO$_4$, 500 mM NaCl, 20 mM imidazole at pH 7.5) supplemented with 1 mM PMSF, 1 mM benzamidine, 5 μg/ml leupeptin and 70 μg/ml pepstatin. The cell suspension was passed through a French press at 20 000 lbs/in^2 pressure four consecutive times and the lysate was spun for 45 min

at 30 000g in a Beckman MLA-80 rotor to clear cell debris and loaded at a flow rate of 0.5 ml/min into a HisTrap HP column (GE Healthcare) previously equilibrated with binding buffer. Nonspecifically bound proteins were washed by running additional binding buffer and RbgA was subsequently eluted from the column with an imidazole gradient from 20 to 600 mM. Fractions of 0.5 ml were collected and those corresponding to RbgA were pooled and diluted with 20 mM Na$_2$HPO$_4$, 5% glycerol at pH 7.5 until the concentration of NaCl reached 100 mM. Any precipitated protein was removed by spinning the protein solution for 10min at 12 000g in a Beckman Coulter Allegra centrifuge. The supernatant was loaded on to a Hi Trap SP HP column (GE healthcare) equilibrated in 20 mM Na$_2$HPO$_4$, 100 mM NaCl, 5% glycerol at pH 7.5 using a flow rate of 1 ml/min. After washing the column with the same buffer, proteins were eluted with a NaCl gradient from 100 mM to 1 M. Fractions containing protein were verified by SDS-PAGE pooled and supplemented with 1.5 mM MgCl$_2$ and 1 mM GMPPNP (only for MST experiments), protease inhibitors (Complete EDTA-Free, Roche), and 20% glycerol. Finally, protein concentration was measured and fractions were aliquoted and frozen in liquid nitrogen for storage at −80°C.

Purification of ribosomal particles from IF2- and RbgA-depleted strains

To purify the mature 50S subunits and $45S_{RbgA}$ particles, strains were first grown at 37°C on LB agar plates supplemented with 5μg/ml chloramphenicol and 1mM IPTG. The depletion was initiated by resuspending some colonies in 100 ml of pre-warmed LB medium containing 5μg/ml chloramphenicol (initial OD$_{600}$ ∼ 0.01–0.02) and grown to OD$_{600}$ ∼0.4–0.5 at 37°C. This culture was then used to inoculate 600 ml of fresh pre-warmed media to reach an initial OD$_{600}$ of ∼0.02–0.04 and then incubated at 37°C with agitation. To minimize the probability of genetic suppressors arising, the culture was harvested when cells reached a doubling time between 140 and 150 min corresponding usually to A_{600} ∼0.3–0.4.

In the case the 50S subunits and $45S_{RbgA}$ particles that were used for the microscale thermophoresis experiments (MST) cells were harvested by centrifugation for 20 min at 3000g in a Beckman JLA-8.1000 rotor and washed with 30 mL of PBS buffer. The cell pellet was then resuspended in buffer A$_{MST}$ (20 mM Tris–HCl pH 7.5, 60 mM NH$_4$Cl, 10 mM Mg acetate, 0.5 mM EDTA, 3 mM β-mercaptoethanol, complete EDTA-free protease inhibitors (Roche) and 20 μl RNase-free DNase (Roche)). Cells were lysed by four consecutive passes through a French press set at 20 000 lbs/in^2. The cell lysate was then centrifuged at 32 000g for 40 min in a MLA-80 rotor to clear cell debris. The clarified lysate was layered over a 1.1 M sucrose cushion of equal volume in buffer B$_{MST}$ (20 mM Tris–HCl at pH 7.5, 60 mM NH$_4$Cl, 10 mM Mg acetate, 0.5 mM EDTA, 3mM β-mercaptoethanol) and centrifuged for 16 h at 110 000g in a Beckman MLA-80 rotor. The ribosomal pellet was washed by buffer C$_{MST}$ (20 mM Tris–HCl (pH 7.5), 60 mM NH$_4$Cl, 10 mM Mg acetate, 0.5 mM EDTA and 7mM β-mercaptoethanol) under gentle agitation before pelleted again by centrifugation

for 16 h at 110 000g with MLA-80 rotor. The ribosomal pellet was then resuspended in buffer E_{MST} (10 mM Tris–HCl pH 7.5, 15 mM Mg acetate, 60 mM NH_4Cl, 3 mM β-mercaptoethanol). Approximately 300 A_{260} units of resuspended crude ribosomes were then loaded at the top of a 35 ml 36–86% (w/v) sucrose density gradients equilibrated in buffer E_{MST} and centrifuged for 14 h at 60 000g in a Beckman SW 32 Ti rotor. Gradients were then fractionated on an AKTAprime FPLC system (GE Healthcare Life Sciences) by monitoring UV absorbance at 254 nm. Fractions corresponding to ribosomal subunits of interest were pooled and pelleted by centrifugation for 16 h at 110 000g in a Beckman MLA-80 rotor. The ribosomal subunit pellets were solubilized in buffer E_{MST}, quantified, frozen in liquid nitrogen and stored at −80°C.

To purify the $45S_{RbgA}$ particles that were used for the cryo-EM experiments the cell pellets were resuspended using 10 ml buffer A_{Cryo} (10 mM Tris–HCl pH 7.5, 10 mM $MgCl_2$, 60 mM KCl, 1 mM DTT) with 0.5% Tween, one-fourth of protease inhibitor cocktail tablet (Roche) and 20 μl DNase I (Roche). Cells were lysed by three consecutive passes through a French press set at 20 000 lbs/in^2. The lysate was clarified by centrifugation at 30 000g for 45 min using a Beckman MLA80 rotor. The supernatant was overlaid on a 1.1 M sucrose cushion on buffer B_{Cryo} (20 mM Tris–HCl pH 7.5, 10 mM $MgCl_2$, 50 mM NH_4Cl, 1 mM DTT) of equal volume and centrifuged at 172 000g for 2.5 h using a Beckman MLA80 rotor. The pellet obtained was resuspended in buffer C_{Cryo} (10 mM Tris–HCl pH 7.5, 10 mM $MgCl_2$, 500 mM NH_4Cl, 2 mM 2-mercaptoethanol) and centrifuged for 2.5 h at 172 000g in a Beckman MLA80 rotor. The resulting pellet was resuspended with buffer B_{Cryo}, which was loaded onto a 34 ml 10–30% (w/v) sucrose gradient made with buffer B_{Cryo}. Approximately 50–60 A_{260} units of crude ribosome of 0.5–0.7 ml volume were loaded on each of these gradients and centrifuged at 35 500g for 16 h in a Beckman SW 32 Ti rotor. The fractions corresponding to the 45S particles in the gradient were collected, pooled and centrifuged for 16 h at 100 000g in a Beckman MLA-80 rotor. The 45S pellet was resuspended in 150μl buffer B_{Cryo}, flash frozen with liquid nitrogen and stored at −80°C for later use in the cryo-EM experiments.

Microscale thermophoresis

Before performing the MST experiment, all RbgA and ribosomal particles samples were spun at 14 000g for 10 min to remove any aggregates. All dilutions were done in 0.5 ml Protein LoBind Eppendorf tubes. RbgA protein was first fluorescently labeled with NHS red on lysine residues using the Monolith NT™ Protein Labeling Kit. The labeling reaction was performed according to the manufacturer's protocol by mixing RbgA at a final concentration of 20 μM protein with a 3-fold molar excess of dye at room temperature for 30 min in the dark. The provided labeling buffer was supplemented with 10 mM Mg acetate. Free dye was eliminated using the Gravity Flow Column B pre-equilibrated with 20 mM Tris–HCl pH 7.5, 250 mM NaCl, 10 mM $MgCl_2$, 2 mM DTT and 0.05% Tween 20.

We then prepared a 120 nM solution of labeled RbgA in MST buffer (10 mM Tris–HCl pH 7.5, 60 mM NH_4Cl,

15 mM Mg acetate, 1 mM DTT, 0.05% Tween 20) and we supplemented it with 1 mM GMPPNP. We then made a 1:1 serial dilution with 16 tubes in MST buffer with ribosomal subunits (50S or 45S). The highest concentration of this serial dilution was 4 μM. To perform the MST experiment, 10 μl of each ligand dilution was mixed 1:1 (v/v) with the labeled RbgA, yielding a final RbgA concentration of 60 nM and from 2 μM to 0.061 nM of ribosomal particles along the dilution series. All reactions were incubated for 10 min at room temperature before loading them into premium glass capillaries (NanoTemper Technologies). MST measurements were performed using the Monolith NT.115 microscale thermophoresis instrument (NanoTemper Technologies) at room temperature. Experiments were conducted at LED power of 50% and low MST IR-laser power. The resulting binding curves and dissociation constants (K_d) were obtained by plotting the normalized fluorescence (F_{norm} (‰) = F_1/F_0) versus the logarithm of the different concentrations of ribosomal subunits. The obtained K_d values were calculated from three independently performed experiments using the NanoTemper analysis software (version 2.2.6).

Cryo-electron microscopy

To prepare the cryo-EM grids containing the $45S_{RbgA}$ particles, we prepared a dilution of the particles in buffer B_{Cryo} to a concentration of 50 nM and applied it directly to the grid immediately right after the dilution step. To prepare the RbgA+$45S_{RbgA}$ complex, we set a 10 μl assembly reaction in buffer B_{Cryo} supplemented with 2 mM GMPPNP containing RbgA and $45S_{RbgA}$ particles at concentrations of 20 and 0.5 μM, respectively. The reaction was then incubated at 37°C for 15 min, diluted 10-fold in buffer B_{Cryo} supplemented with 2 mM GMPPNP and 2 μM RbgA. Then, the reaction was immediately applied to the grid.

Cryo-EM grids were prepared by applying a 3.6 μl volume of the diluted samples to holey carbon grids (c-flat CF-2/2-2C-T) with a freshly applied additional layer of continuous thin carbon (5–10 nm). A glow discharge treatment of 5 mA for 15 s right before the sample solution was applied to the grid. Grid vitrification was performed in a Vitrobot (Thermo Fisher Scientific Inc.). Grids were blotted for 3 s and with a blot force +1 before they were plunged into liquid ethane. The Vitrobot was set at 25°C and 100% relative humidity.

Data collection for the $45S_{RbgA}$ particles (8950 movies) was done at FEMR-McGill core facility using a Titan Krios microscope at 300 kV equipped with a Falcon II direct electron detector (Thermo Fisher Scientific Inc.). EPU software was used for automated data acquisition. Movies for the $45S_{RbgA}$ particles were collected with a total dose of 40 e$^-$/Å^2. All datasets were collected as movies with seven frames acquired in 1 s exposure at a magnification of 75 000×, producing images with a calibrated pixel size of 1.073 Å. The nominal defocus range used during data collection was between −1.25 and −2.75 μm.

Data collection for the RbgA+$45S_{RbgA}$ complex (1228 movies) was collected at the Hospital for Sick Children in Toronto in a FEI Tecnai F20 electron microscope operated at 200 kV. Grids were loaded in a Gatan 626 single tilt cryo-

holder and images were collected with a Gatan K2 Summit direct detector device camera in counting movie mode with five electrons per pixel per second for 15 s exposures and 0.5 s per frame. This method produced movies consisting of 30 frames with an exposure rate of ∼1 e$^-$/Å^2. Movies were collected with a defocus range of 1–2.5 μm and a nominal magnification of 25 000×, which produced images with a calibrated pixel size of 1.45 Å.

Image processing

The datasets for both the 45S$_{RbgA}$ particles and RbgA+45S$_{RbgA}$ complex were processed using the same processing pipeline. Movies for corrected for beam induced motion correction and their CTF parameters estimated using MotionCor2 (24) and Gctf (25) programs. Subsequent processing steps were done with Relion 2.1 program (26) and Relion-3 (27). The auto-picking step produced 1,588,691 particle images in the case of the 45S$_{RbgA}$ dataset and 182 534 for the RbgA+45S$_{RbgA}$ dataset. Both datasets were cleaned up using reference-free 2D classifications. A total of 1 339 712 and 169 095 particles were selected forming the 'clean' datasets, which were then subjected to 3D classifications. The mature 50S subunit from *B. subtilis* (PDB 3J9W) after applying a 60 Å low-pass Fourier filter was used as initial reference for 3D classifications. A mask created from the mature 50S subunit was used for all 3D classification steps in the 45S$_{RbgA}$ dataset. This mask was created using the 'relion_mask_create' command an initial threshold for binarization of 0.04, extension of the binary mask by two pixels and creating a soft-edge with a width of two pixels. No mask was used for the RbgA+45S$_{RbgA}$ dataset. Resulting maps from the 3D classification procedures were visually inspected and those particles assigned to classes representing the same structure were merged for refinement. The initial map used as initial reference in the refinement procedures for those classes presenting a formed central protuberance was the mature 50S subunit from *B. subtilis* (PDB 3J9W) after applying a 50 Å low-pass Fourier filter. To refine those classes with absent central protuberance, we used one of the intermediate cryo-EM maps obtained during classification in which this structural motif was not present. A 50 Å low-pass Fourier filter was also applied in this case.

Sharpening of the cryo-EM maps and local resolution analysis of the structures was done was also done using Relion (28).

Map analysis and atomic model building

Difference map analysis of the RbgA+45S$_{RbgA}$ complex was done using relion_image_handler command from Relion-3 (27). First both maps were low pass filtered to 15 Å and brought to a similar power spectra. Subsequently the two maps were subtracted to produce the difference map.

To build the atomic model for the 45S$_{RbgA}$ particle and RbgA+45S$_{RbgA}$ complex, we first used Chimera (29) to fit by rigid-body docking the atomic model of the mature 50S subunit (PDB 3J9W) and RbgA (PDB 1PUJ) into the cryo-EM density maps. These initial models were improved by rounds of real space refinement using Phenix (30) and manual model building in Coot (31,32). The connectivity of the

cryo-EM maps was improved using the automatic sharpening tool phenix.auto_sharpen (33), which is available as part of the PHENIX software suite (34). Elements of rRNA or r-proteins present in the atomic model of the 50S subunit or RbgA crystal structure but absent from the cryo-EM maps of the 45S$_{RbgA}$ particle and RbgA+45S$_{RbgA}$ complex are not included on the final models.

Figures for this manuscript were prepared using Pymol program (The PyMOL Molecular Graphics System, Version 1.2r3pre, Schrödinger, LLC), UCSF Chimera and Chimera X (29).

RESULTS

High resolution structure of the 45S$_{RbgA}$ particle accumulating in RbgA-depleted cells

To visualize the conformational changes that RbgA induces upon binding to the 45S$_{RbgA}$ particle, we solved the cryo-EM structure (Figure 1C) of this assembly intermediate after purification (Figure 1A). We found that the immature 45S$_{RbgA}$ particles accumulating in RbgA-depleted cells are arrested mainly at two distinct maturation steps (class A and class B). The distribution of particles between class A and B was 51% and 49%, respectively. We produced a cryo-EM map from each group of particles (Figure 1C and Movies 1 and 2) and both refined to 3.4 Å resolution (Supplementary Figure S1). Previous cryo-EM maps for the 45S$_{RbgA}$ particle were limited to ∼10 Å resolution (16,17).

We then compared the structure of the immature 45S$_{RbgA}$ particles to the structure of the mature 50S subunit (Figure 1B). The two structures exhibited a well-resolved core region, similar to the mature 50S subunit. However, the L7/12 stalk (H42-H44) (Figure 1C and Movies 1 and 2) and functional rRNA helices in the A, P and E sites were invisible indicating these regions are still in an immature state in both class A and B intermediates. In particular, we found that none of the cryo-EM maps had significant density corresponding to H38 (A-site finger) and H42-44 (Supplementary Figure S2A) or for H89 and H91-92 in the A site (Supplementary Figure S2B). In addition, there was also no density for H69, H71 (Supplementary Figure S2C) and H93 (Supplementary Figure S2B) that together form the P site or the long H68 (Supplementary Figure S2C), an important structural component of the E site. Similar to other structures representing 50S subunits, the L1 (H76-H78) stalk was also not visible due to the intrinsic flexibility of this rRNA motif even in the mature subunit. The most noticeable differences between the class A and class B assembly intermediates was the central protuberance (CP). In the cryo-EM map for class B particles, all of the rRNA helices forming the CP (H80-88) were developed but none of them were visible in the cryo-EM map for class A (Supplementary Figure S2D).

Using the cryo-EM maps, we produced molecular models for class A and B assembly intermediates (Supplemental Table S1) and used these models to produce temperature maps that measured how much the rRNA regions present in these structures deviated from the conformation of the mature 50S subunit (Supplementary Figure S3). The pattern emerging was that the core region showed the highest degree of similarity with the mature structure and the CP
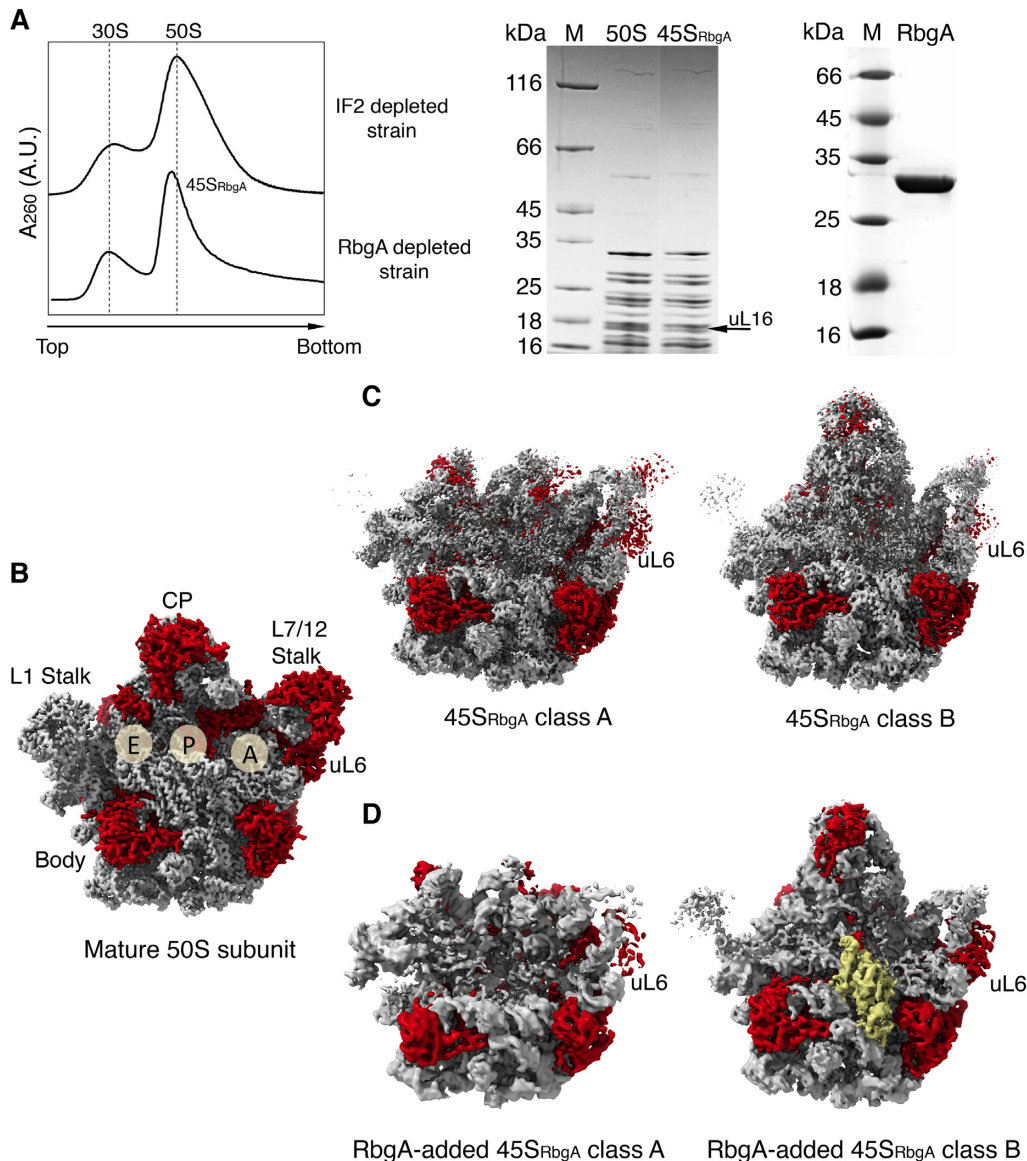
Figure 1. Cryo-EM structure of the 45S$_{RbgA}$ particle and the RbgA+45S$_{RbgA}$ complex. (**A**) Purification of ribosomal particles. Mature 50S subunits and 45S$_{RbgA}$ particles were purified using sucrose gradient ultracentrifugation. The left panel shows the ribosome profiles from *B. subtilis* strains depleted from IF2 (that accumulate 50S subunits) and RbgA accumulating 45S$_{RbgA}$ particles. Vertical lines indicate where the 30S and 50S mature particles migrate in the gradient. Middle panel shows purified 50S and 45S$_{RbgA}$ particles resolved in a SDS-PAGE and stained with Coomassie brilliant blue. The right panel shows purified RbgA protein also resolved in a Coomassie brilliant blue stained SDS-PAGE. (**B**) Map of the mature 50S subunit shown for comparison purposes. This map was obtained by applying a low pass filter of 4 Å to the atomic model of the 50S subunit from *B. subtilis* (PDB ID: 3j9w). The rRNA is colored in grey and the r-proteins are shown in red. Important landmarks of the structure are labeled including the A, P and E sites (yellow circles). (**C**) Cryo-EM maps of the two conformers found for 45S$_{RbgA}$ particles. (**D**) Cryo-EM maps obtained for the two conformers found in an assembly reaction containing RbgA and 45S$_{RbgA}$ particle. Class B showed an additional density attached to the P site corresponding to RbgA (colored in yellow).

and existing structural motifs in the subunit stalk and the A, P and E functional sites exhibited the highest degree of divergency.

Previous quantitative mass spectrometry analysis of 45S$_{RbgA}$ particles (17) found that these ribosomal particles are severely depleted from uL16, bL27, bL28, bL33, bL35 and bL36 r-proteins. Most of these r-proteins are located at the base of the CP (Supplementary Figure S4A). Densities corresponding to these r-proteins were also missing from the cryo-EM map of class A (Supplementary Figure S4B). In addition, there were five other r-proteins (uL10, uL11 in

the bL7/L12 stalk and uL5, bL31 and uL18 in the central protuberance) that were present at ∼100% occupancy according to qMS (17), but density corresponding to these proteins was also completely missing in the map for class A (Supplementary Figure S4B). This observation suggests these r-proteins are bound to the assembly intermediate in a flexible manner. The map for class B with a well-formed CP also missed the densities for all these r-proteins, except bL27 and uL18, which presented a well-defined density. Finally, density for uL6 was present but highly fragmented in the

maps of both classes (Figure 1C and Supplementary Figure S4C).

RbgA binds the immature 45S$_{RbgA}$ particles with high affinity

We measured the dissociation constants (K_d value) of RbgA binding to the immature 45S$_{RbgA}$ particles and to the mature 50S subunits in the presence of GMPPNP using microscale thermophoresis (MST) (35,36). In these experiments, the thermophoretic mobility of fluorescently labeled RbgA was measured at increasing concentration of ribosomal particles. We found that the K_d value of the assembly factor for the immature particle was ∼93.4 ± 3.1 nM, whereas this value increased by an order of magnitude to ∼1.06 ± 0.3 μM when measured against the mature 50S subunit (Figure 2A). These measurements indicated that in the presence of GMPPNP, RbgA exhibits higher affinity for the 45S$_{RbgA}$ particle than for the mature 50S subunit.

RbgA binds the P-site of 45S$_{RbgA}$ particles and stabilizes rRNA helices in the A and P functional sites

To visualize the binding of RbgA to the 45S$_{RbgA}$ particles, we incubated RbgA and 45S$_{RbgA}$ particles in the presence of GMPPNP. This reaction was studied by cryo-EM and single particle analysis. Similar to the control sample containing 45S$_{RbgA}$ particles without RbgA added, we found that this sample also contained class A and class B type of assembly intermediates (Figure 1D). The map for class A and class B refined to resolutions of 5 Å and 4.4 Å, respectively (Supplementary Figure S5). In the RbgA-added sample, Class B particles exhibited a fully developed CP and a clear density representing RbgA attached to the P site (Figure 1D, right panel and Movie 3). We called this map the RbgA+45S$_{RbgA}$ complex. Class B particles accounted for a 57% of the population. The remaining 43% were class A particles (Figure 1D; left panel) and they did not show a density corresponding to the CP or RbgA. These results indicate that RbgA targets only class B particles for binding.

Next, we built a molecular model for the RbgA+45S$_{RbgA}$ complex to identify the regions in the factor and the assembly intermediate important for the interaction. We found that the two domains of RbgA make extensive contacts with the rRNA of the ribosomal subunit (Figure 2B). However, the only protein-protein interactions observed was that between the C-terminal domain of RbgA and r-protein uL14 (Figure 2C). RbgA binds to the ribosomal particle by embedding its N-terminal GTPase domain into the location that H69 and H71 occupy in the mature subunit (Figure 2D). In doing so, RbgA displaces these two helices in the P-site and interacts with several surrounding helices, including H92 and H93. The C-terminal helical domain sits right below interacting mainly with H62 and H64 (Figure 2B).

Binding of RbgA triggers a number of dramatic conformational changes in the 45S$_{RbgA}$ particle (Figure 3 and Movie 4). This included stabilization of the rRNA helices H91-92 in the A site, H93 in the P site and the partial stabilization of H38. Density for all of these rRNA helices became apparent and adopted a mature conformation (Figure 3A). The L1 stalk (H76-78) also became partially visible upon RbgA binding, but still appeared as a fragmented

density similarly to the structures of the mature 50S subunit. However, the functional rRNA helices H89 in the A site, H69 and H71 in the P site and the long helix H68 paving the floor of the tRNA passage from the PTC to the E site remained flexible upon RbgA binding and were not visible in the map of the RbgA+45S$_{RbgA}$ complex (Figure 3A).

A difference map calculated between the cryo-EM map of the RbgA+45S$_{RbgA}$ complex and the 45S$_{RbgA}$ particle class B (Figure 3B) showed differential densities matching in location the r-protein uL6 and the rRNA helices stabilized upon RbgA binding (Figure 3C). In addition, the difference map showed a number of scattered densities mainly localized in the central protuberance area caused by the conformational differences existing in this region between the structure of the RbgA+45S$_{RbgA}$ complex and that of the 45S$_{RbgA}$ particle class B (Figure 3B). Consistent with these results, we calculated a temperature map to measure how much the rRNA regions in the RbgA+45S$_{RbgA}$ complex and 45S$_{RbgA}$ particle class A and B deviated from the conformation of the mature 50S subunit. This map revealed that RbgA binding had an overall stabilizing effect in the regions of the 23S rRNA forming the CP (h80-88) (Supplementary Figure S3).

Density for the r-proteins found depleted or absent by qMS (uL16, bL28, bL33, bL35 and bL36) (17) were also missing in the cryo-EM map of the RbgA+45S$_{RbgA}$ complex (Supplementary Figure S6). The other r-proteins that showed a highly fragmented density or no density at all due to their high flexibility in the 45S$_{RbgA}$ particle (uL10, uL11 and bL31) (Supplementary Figure S6), were also not visible in the cryo-EM map of the RbgA+45S$_{RbgA}$ complex either. However, density for r-protein uL6 exhibiting a highly fragmented density in the free 45S$_{RbgA}$ particle cryo-EM maps (Supplementary Figure S4B and S4C) became well defined upon RbgA binding (Supplementary Figure S6). This observation suggests that RbgA has a stabilizing effect on the binding of uL6.

Taken together the cryo-EM structure of the RbgA+45S$_{RbgA}$ complex allowed us to visualize the cascade of conformational changes that the binding of RbgA causes upon binding in the 45S$_{RbgA}$ particle.

Conformational changes in RbgA upon binding to the 45S$_{RbgA}$ particle

Previous crystallographic work has produced the crystal structures of RbgA from *T. maritima* (11), *B. subtilis* (PDB 1PUJ) and *S. aureus* (18). These structures were obtained bound to different guanidine nucleotide, including GDP, GTP, GNP, GMPPNP and the alarmone molecules ppGpp and pppGpp (Figure 4A). Our cryo-EM structure was prepared in large molar excess of GMPPNP and the structure reflects full occupancy of this non-hydrolysable nucleotide at the nucleotide binding site of RbgA (Figure 4B). None of the crystallographic structures are in complex with rRNA. Therefore, to visualize the conformational changes that RbgA undergoes upon binding to the 45S$_{RbgA}$ particle, we compared the 45S$_{RbgA}$-bound structure of RbgA obtained by cryo-EM with these RNA-free RbgA structures (Figure 4A).
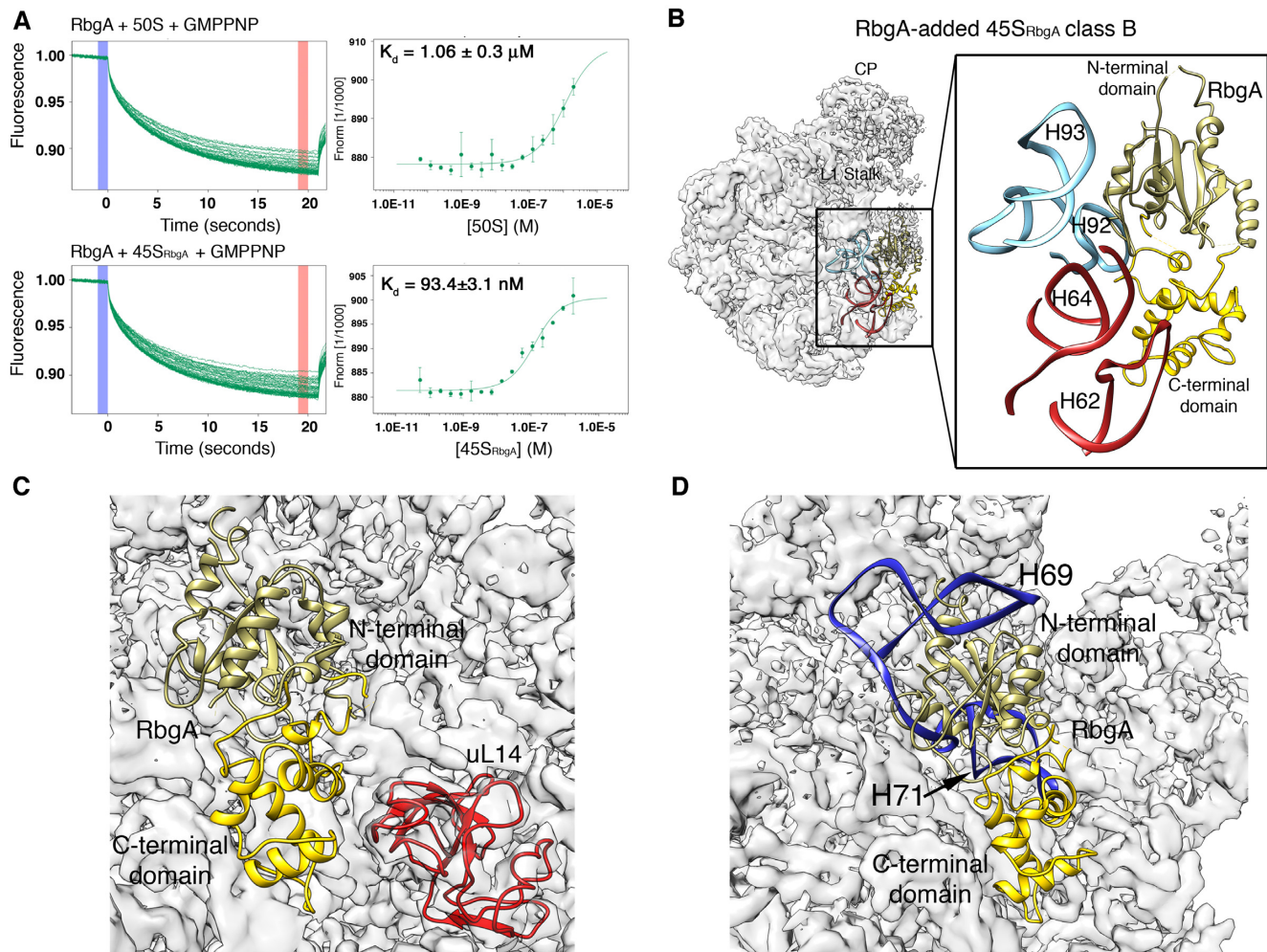
Figure 2. Binding of RbgA to the 45S$_{RbgA}$ particle. (**A**) Measurement of the binding affinity of RbgA to the immature 45S$_{RbgA}$ particle and mature 50S subunit by MST. Fluorescence time traces are shown in the left panels and derived F_{norm} (‰) $= F_1/F_0$ curves for the two binding reactions are shown in the right panels. (**B**) Side view of RbgA+45S$_{RbgA}$ complex cryo-EM map (left panel). The framed area is shown as a zoomed in view in the right panel. The 23S rRNA helices important for the binding of the N-terminal and C-terminal domains of RbgA to the 45S$_{RbgA}$ particle are labeled and colored in cyan and red, respectively. The N-terminal and C-terminal domains of RbgA are colored in gold and yellow, respectively. (**C**) Zoomed in view of the RbgA binding region in the 45S$_{RbgA}$ particle. RbgA and r-protein uL14 (in red) near to the binding region are shown in ribbon representation. RbgA N-terminal and C-terminal domains are color coded as in panel (B). (**D**) Zoomed in view of the RbgA binding region showing how the N-terminal domain of the assembly factor sits in the place that rRNA H69 and H71 occupy in the mature subunit.

The crystal structures already showed that the overall conformation of RbgA and orientation of the two domains remains almost the same, despite which nucleotide is bound to the protein. Comparison with our 45S$_{RbgA}$-bound RbgA structure also revealed that its overall conformation does not dramatically change upon binding to the ribosomal particle (Figure 4A). The highest degree of similarity was observed with the GNP-bound RbgA from *B. subtilis* (PDB 1PUJ) indicated by a root-mean-square deviation (r.m.s.d.) value of 1.1. Comparison with the other structures from S. *aureus* (18) and *T. maritima* (11) produced a r.m.s.d. value of ∼1.2, regardless of the nucleotide state.

Interaction of highly conserved regions in RbgA with the 45S$_{RbgA}$ particle

In RbgA, the G4 (Leu57-Asp61) and G1 (Gly127-Thr135) motifs surround the binding site for the guanidine nu-

cleotide, located in the concave side of RbgA (Supplementary Figure S7), also interact with the 23S rRNA in the 45S$_{RbgA}$ particle. The G2 motif (Gly153-Thr155) includes the switch I region. This region is disordered in all the unbound RbgA X-ray structures, but it becomes ordered upon binding to the 45S$_{RbgA}$ particle (Figure 4D). Finally, the G3 motif (Asp171-Gly174) includes the switch II region and forms a loop connecting the GTPase with the C-terminal domain. The location of switch II does not differ dramatically in the 45S$_{RbgA}$-bound RbgA structure compared to the equivalent region in the unbound *B. subtilis* RbgA structure (PDB 1PUJ) (Figure 4A).

RbgA also contains four highly-conserved regions designated CR1 to CR4 (12). CR1 (Ile3-Val17) and CR2 (Asp32-Pro42) are contained in the GTPase domain preceding the circularly permuted G-motifs, whereas CR3 (Thp177-Asp182) and CR4 (Arg188-Asp197) regions are right af-
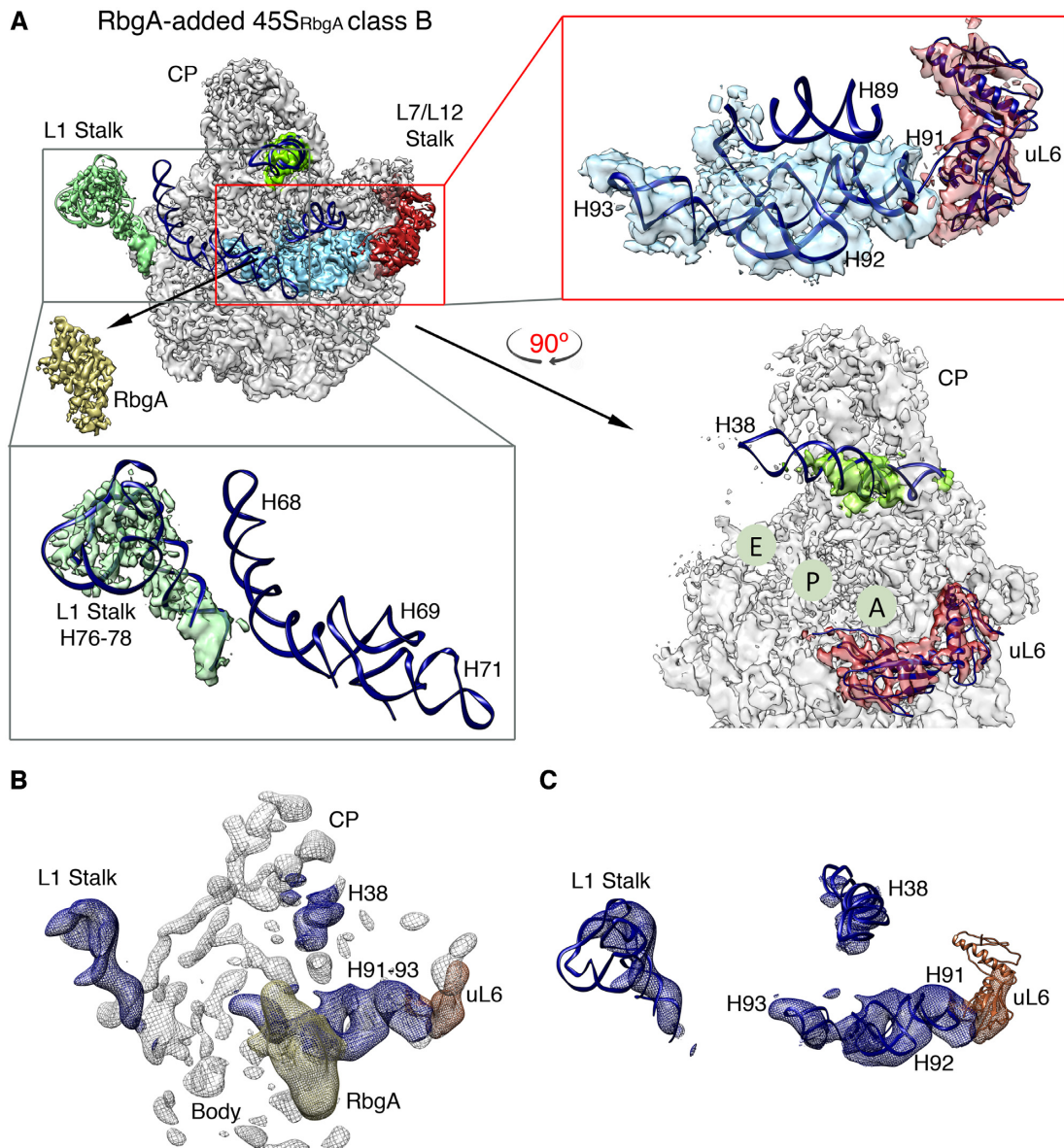
Figure 3. Conformational changes induced upon RbgA binding to the 45S$_{RbgA}$ particle. (**A**) Overview of the RbgA+45S$_{RbgA}$ complex cryo-EM map (top-left panel). RbgA was segmented and computationally removed for easy visualization of the A, P and E sites. Boxes demark the areas where conformational changes are observed. Bottom-left and top-right panel show zoomed in views of the framed areas. The bottom-right panel shows a side view of the RbgA+45S$_{RbgA}$ complex cryo-EM map with the densities for H38 and uL6 colored in fluorescent green and sienna colors, respectively. The A, P and E functional sites are labeled. The atomic model of the mature 50S subunit (PDB ID 3j9w) was fitted to identify relevant structural motifs in the cryo-EM map. (**B**) Difference map analysis of the RbgA+45S$_{RbgA}$ complex. The cryo-EM map of the 45S$_{RbgA}$ particle class B was subtracted from the cryo-EM map of the RbgA+45S$_{RbgA}$ complex to produce the difference map shown in the panel (white and colored densities). Densities relevant and revealing significant conformational changes in the rRNA and r-protein uL6 induced by RbgA binding are colored in dark blue and sienna. Density corresponding to RbgA is shown in dark gold. Densities are labeled according to the structural motifs from the mature 50S subunit colocalizing with those densities. (**C**) This panel show the colored densities in (B) (except density corresponding to RbgA) segmented out from the entire difference map. The molecular model of the mature 50S subunit (PDB ID 3j9w) was fitted to identify the relevant structural motifs in the difference map.

ter the G3 motif forming a long loop connecting the N and C-terminal domain. The four regions are visible in our cryo-EM map and were included into the molecular model built for the RbgA+45S$_{RbgA}$ complex (Supplementary Figure S7).

The CR1 region is of particular interest for RbgA's GTPase activity. This region is unstructured in all the available RbgA X-ray structures, but visible in our cryo-EM map

(Figure 4B and D). The interaction of the CR1 region with helix 92 of the 23S rRNA in the 45S$_{RbgA}$ particle (Figure 4B) stabilizes this structural motif and places His9 in the vicinity of the γ-phosphate of the guanidine nucleotide explaining how this amino acid act as the key catalytic residue (12). Phe6 is also a highly conserved residue in the CR1 region. The cryo-EM map shows that Phe6 form a hydrophobic interaction with Ile195 in the CR4 domain suggesting
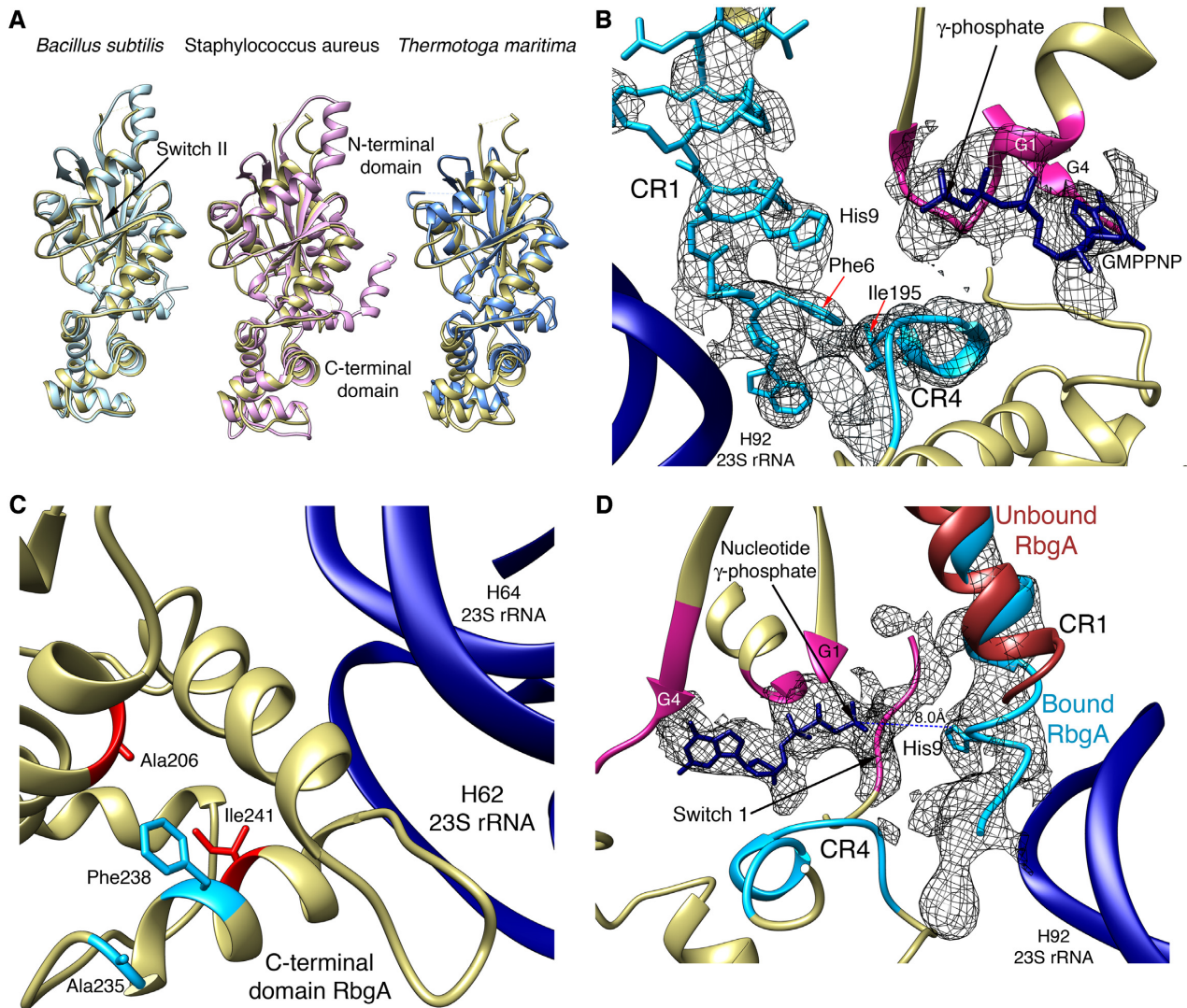
Figure 4. Conformational changes in RbgA upon binding to the 45S$_{RbgA}$ particle. (**A**) Overlap of the atomic model of the 45S$_{RbgA}$ particle bound RbgA derived from our cryo-EM map with the X-ray structures of RNA-free RbgA protein from several microorganism. The 45S$_{RbgA}$ particle bound RbgA (ligand GMPPNP) is represented in golden color in the three panels. The RNA-free RbgA proteins are represented with different colors and they were prepared using PDB files from *B. subtilis* 1PUJ (left) (ligand GMPPNP), *S. aureus* 6G12 (middle) (ligand GMPPNP) and *T. maritima* 3CNL (right) (ligand GNP). (**B**) Zoomed in view of the N-terminal nucleotide binding regions of RbgA. The cryo-EM density map for these regions is shown and the derived molecular model is shown within the density. Highly conserved CR1 and CR4 regions and G1 and G4 motifs of RbgA are labeled and colored in sky blue and pink, respectively. H92 of the 23S rRNA is shown in dark blue. Density and molecular model for switch 1 has been removed from the image for clarity. (**C**) C-terminal domain in the 45S$_{RbgA}$ particle bound RbgA. Helices 62 and 64 of the 23S rRNA in the 45S$_{RbgA}$ particle interacting with the C-terminal domain are shown. Residues Ala206 and Ile241, mutation of which causes bacterial growth defects are shown in stick and indicated in red. The two other highly conserved residues, Ala235 and Phe238 are labelled and highlighted in cyan. (**D**) The interaction of the CR1 region of RbgA (in blue) with helix 92 of the 23S rRNA in the 45SRbgA particle stabilizes this structural motif and places His9 in the vicinity of the γ-phosphate of the guanidine nucleotide explaining how this amino acid could act as the key catalytic residue. The distance between His9 and the γ-phosphate is indicated by a dashed line. Switch I and the associated density is shown running between the catalytic residue and the γ-phosphate, hindering the role of His9 as the catalytic residue. The CR1 region is not visible in the available structures of RNA-free RbgA (colored in sienna). However, this region is visible in 45S$_{RbgA}$ particle bound RbgA and the cryo-EM density for the CR1 region and for the GMPPNP molecule bound to the protein is shown. Other important functional (G1 and G4 motifs) and highly conserved regions (CR4) of RbgA are indicated.

that Phe6 is also an important residue to correctly positioning the CR1 region for efficient GTP hydrolysis (Figure 4B).

In the C-terminal domain of RbgA, there are only four highly conserved residues. These are Ala206, Ala235, Phe238 and Ile241, however only mutations in Ala206 and Ile241 causes severe bacterial growth defects and rendered the factor unable to associate with the large ribosomal sub-unit (12). The cryo-EM structure shows that Ala206 and Ile241 do not mediate interactions with the 23S rRNA in the 45S$_{RbgA}$ particle (Figure 4C) concluding that mutations in Ala206 and Ile241 cause deleterious functional phenotypes (12) likely due to the involvement of these residues in stabilizing the structural fold of the C-terminal domain.

DISCUSSION

Biogenesis of ribosomes from bacteria to humans requires GTPases for accuracy and efficiency. However, their specific roles in the assembly process remain poorly understood ([1–3]). RbgA is an essential GTPase involved in the assembly of the large subunit of the ribosome. Data presented here show that RbgA stabilizes functionally important helices in the 23S rRNA at the A and P sites and the binding of r-protein uL6. In this context, RbgA seems to be required for the A and P sites to reach their mature conformation in the 50S subunit.

Previous chemical probing analysis of the $45S_{RbgA}$ particle ([17]) found no increased reactivity for any of the rRNA helices stabilized by RbgA binding (H91–93 in the A and P site), suggesting that these helices are already formed in the $45S_{RbgA}$ particle but adopt multiple conformations. Other rRNA helices, including H89 (A site), H71 and H69 (P site), which were not stabilized by RbgA binding are also folded in the $45S_{RbgA}$ particles, but they remain invisible in the cryo-EM map of the RbgA+$45S_{RbgA}$ complex due also to their multiple conformations. Instead, H68 (E site) and H42-43 (GTPases associated region) that also remained invisible upon RbgA binding showed a dramatically increased reactivity in the chemical probing experiments with the $45S_{RbgA}$ particle suggesting they were unfolded in the immature particle. Therefore, our data along with the previous chemical probing analysis of the $45S_{RbgA}$ particle ([17]) indicates that RbgA binding stabilizes helices H91–93 and H76–78 in the 23S rRNA of the $45S_{RbgA}$ particle, but not their folding.

The cryo-EM map of the RbgA+$45S_{RbgA}$ complex suggests a model to explain how His9 in the CR1 region of RbgA may function as the catalytic residue during GTP hydrolysis, and provides an structural explanation for previously reported measurements of RbgA GTPase activity ([13–15]). The CR1 region is flexible when RbgA is not in complex with the ribosomal subunit (Figure [4]D) ([11,18]) explaining the low intrinsic GTPase activity of the protein. Interaction of RbgA with H92 of the 23S rRNA in the $45S_{RbgA}$ particle stabilizes the CR1 region, placing His9 in the vicinity of the γ-phosphate of the guanidine nucleotide that may then act as the key catalytic residue during GTP hydrolysis (Figure [4]B). However, in the cryo-EM map of the RbgA+$45S_{RbgA}$ complex, the distance between His9 and the γ-phosphate is 8 Å (Figure [4]D), which is longer than optimal for effective GTP hydrolysis ([37,38]). In addition, switch I runs between the catalytic residue and the γ-phosphate hindering its involvement in hydrolysis (Figure [4]D). This structural arrangement correlates with biochemical data ([13–15]) showing that in the presence of immature $45S_{RbgA}$ particles, RbgA only achieves partial stimulation of its GTPase activity. Maximal stimulation of RbgA GTPase activity occurs in the presence of the mature 50S subunits, but a structure of RbgA bound to the mature subunit for comparison is yet to become available. However, by analogy with other GTPase structures associated with ribosomal function ([37,38]), we predict that when RbgA binds to the mature subunit, His9 and the entire CR1 region will be closer (∼4 Å) to the γ-phosphate of the guanidine nucleotide and switch I will not be blocking their interaction.

A suppressor study has provided evidence for a functional interaction between RbgA and r-protein uL6 during assembly ([39]). This study showed that the growth defect caused by mutating Phe6 to Ala in RbgA (RbgA-F6A) is partially suppressed by compensatory mutations in the N-terminal region of uL6, which contact helix 97 in the 23S rRNA. How these compensatory mutations in uL6 suppress the lack of RbgA function cannot be explained from our cryo-EM structure. However, the work presented here explains how this functional interaction is implemented. Upon binding to the $45S_{RbgA}$ particle, RbgA stabilizes multiple rRNA helices in the A and P sites that span the space between the binding site of RbgA and uL6. Once these rRNA helices adopt the mature conformation, the two main anchor points for uL6 including helix H97 and the sarcin/ricin loop (H95) become stable and provide a firm binding site for the protein. Consequently, uL6 goes from exhibiting a fragmented density in the structure of the $45S_{RbgA}$ particle (Figure [1]C and Movies 1 and 2) to a well-defined density in the structure of the RbgA+$45S_{RbgA}$ complex (Figure [1]D and Movie 3).

The cryo-EM map of the $45S_{RbgA}$ particles described here present a remarkable similarity to the $45S_{YphC}$ and $44.5S_{YsxC}$ particles that accumulate in *B. subtilis* cells upon depletion of YphC and YsxC, two additional GTPases involved in the maturation of the 50S subunit ([15]). These immature ribosomal subunits also present the same functionally important rRNA helices in the A, P and E site in a non-native conformation. Importantly, RbgA, YphC and YsxC bind to all these immature particles and simultaneous binding of these factors to these assembly intermediates is also possible ([15]). However, whether they work in conjunction or sequentially in the cell to assist the maturation of the 50S subunit still remains a question. It is likely that YphC and YsxC and/or other r-proteins may be necessary to visualize additional RbgA dependent maturation steps or further stabilize the conformational changes described from this work.

Another unclear aspect of RbgA functionality is the observation that most organisms ranging from bacteria to humans require RbgA to form ribosomes, whereas many proteobacteria including *Escherichia coli* have lost this requirement ([1]). Future work will uncover this and other questions that still remain regarding the role of RbgA and other assembly factors, including YphC and YsxC in the assembly of the large ribosomal subunit.

DATA AVAILABILITY

The cryo-EM maps for the $45S_{RbgA}$ particle class A and class B and the RbgA+$45S_{RbgA}$ complex are deposited in the EMDB with assigned IDs 20491, 20435 and 20441, respectively. The atomic models for these structures were deposited in the Protein Data Bank with assigned IDs 6PVK, 6PPF and 6PPK, respectively.

SUPPLEMENTARY DATA

Supplementary Data are available at NAR Online.

REFERENCES

1. Britton,R.A. (2009) Role of GTPases in bacterial ribosome assembly. *Annu. Rev. Microbiol.*, **63**, 155–176.
2. Karbstein,K. (2007) Role of GTPases in ribosome assembly. *Biopolymers*, **87**, 1–11.
3. Wilson,D.N. and Nierhaus,K.H. (2007) The weird and wonderful world of bacterial ribosome regulation. *Crit. Rev. Biochem. Mol. Biol.*, **42**, 187–219.
4. Matsuo,Y., Morimoto,T., Kuwano,M., Loh,P.C., Oshima,T. and Ogasawara,N. (2006) The GTP-binding protein YlqF participates in the late step of 50 S ribosomal subunit assembly in Bacillus subtilis. *J. Biol. Chem.*, **281**, 8110–8117.
5. Uicker,W.C., Schaefer,L. and Britton,R.A. (2006) The essential GTPase RbgA (YlqF) is required for 50S ribosome assembly in Bacillus subtilis. *Mol. Microbiol.*, **59**, 528–540.
6. Morimoto,T., Loh,P.C., Hirai,T., Asai,K., Kobayashi,K., Moriya,S. and Ogasawara,N. (2002) Six GTP-binding proteins of the Era/Obg family are essential for cell growth in Bacillus subtilis. *Microbiology*, **148**, 3539–3552.
7. Barrientos,A., Korr,D., Barwell,K.J., Sjulsen,C., Gajewski,C.D., Manfredi,G., Ackerman,S. and Tzagoloff,A. (2003) MTG1 codes for a conserved protein required for mitochondrial translation. *Mol. Biol. Cell*, **14**, 2292–2302.
8. Bassler,J., Grandi,P., Gadal,O., Lessmann,T., Petfalski,E., Tollervey,D., Lechner,J. and Hurt,E. (2001) Identification of a 60S preribosomal particle that is closely linked to nuclear export. *Mol. Cell*, **8**, 517–529.
9. Hedges,J., West,M. and Johnson,A.W. (2005) Release of the export adapter, Nmd3p, from the 60S ribosomal subunit requires Rpl10p and the cytoplasmic GTPase Lsg1p. *EMBO J.*, **24**, 567–579.
10. Saveanu,C., Bienvenu,D., Namane,A., Gleizes,P.E., Gas,N., Jacquier,A. and Fromont-Racine,M. (2001) Nog2p, a putative GTPase associated with pre-60S subunits and required for late 60S maturation steps. *EMBO J.*, **20**, 6475–6484.
11. Kim do,J., Jang,J.Y., Yoon,H.J. and Suh,S.W. (2008) Crystal structure of YlqF, a circularly permuted GTPase: implications for its GTPase activation in 50 S ribosomal subunit assembly. *Proteins*, **72**, 1363–1370.
12. Gulati,M., Jain,N., Anand,B., Prakash,B. and Britton,R.A. (2013) Mutational analysis of the ribosome assembly GTPase RbgA provides insight into ribosome interaction and ribosome-stimulated GTPase activation. *Nucleic Acids Res.*, **41**, 3217–3227.
13. Achila,D., Gulati,M., Jain,N. and Britton,R.A. (2012) Biochemical characterization of ribosome assembly GTPase RbgA in Bacillus subtilis. *J. Biol. Chem.*, **287**, 8417–8423.
14. Matsuo,Y., Oshima,T., Loh,P.C., Morimoto,T. and Ogasawara,N. (2007) Isolation and characterization of a dominant negative mutant of Bacillus subtilis GTP-binding protein, YlqF, essential for biogenesis and maintenance of the 50 S ribosomal subunit. *J. Biol. Chem.*, **282**, 25270–25277.
15. Ni,X., Davis,J.H., Jain,N., Razi,A., Benlekbir,S., McArthur,A.G., Rubinstein,J.L., Britton,R.A., Williamson,J.R. and Ortega,J. (2016) YphC and YsxC GTPases assist the maturation of the central protuberance, GTPase associated region and functional core of the 50S ribosomal subunit. *Nucleic Acids Res.*, **44**, 8442–8455.
16. Li,N., Chen,Y., Guo,Q., Zhang,Y., Yuan,Y., Ma,C., Deng,H., Lei,J. and Gao,N. (2013) Cryo-EM structures of the late-stage assembly intermediates of the bacterial 50S ribosomal subunit. *Nucleic Acids Res.*, **41**, 7073–7083.
17. Jomaa,A., Jain,N., Davis,J.H., Williamson,J.R., Britton,R.A. and Ortega,J. (2014) Functional domains of the 50S subunit mature late in the assembly process. *Nucleic Acids Res.*, **42**, 3419–3435.
18. Pausch,P., Steinchen,W., Wieland,M., Klaus,T., Freibert,S.A., Altegoer,F., Wilson,D.N. and Bange,G. (2018) Structural basis for (p)ppGpp-mediated inhibition of the GTPase RbgA. *J. Biol. Chem.*, **293**, 19699–19709.
19. Razi,A., Guarne,A. and Ortega,J. (2017) The cryo-EM structure of YjeQ bound to the 30S subunit suggests a fidelity checkpoint function for this protein in ribosome assembly. *Proc. Natl. Acad. Sci. U.S.A.*, **114**, E3396–E3403.
20. Lopez-Alonso,J.P., Kaminishi,T., Kikuchi,T., Hirata,Y., Iturrioz,I., Dhimole,N., Schedlbauer,A., Hase,Y., Goto,S., Kurita,D. *et al.* (2017) RsgA couples the maturation state of the 30S ribosomal decoding center to activation of its GTPase pocket. *Nucleic Acids Res.*, **45**, 6945–6959.
21. Zhang,X., Yan,K., Zhang,Y., Li,N., Ma,C., Li,Z., Zhang,Y., Feng,B., Liu,J., Sun,Y. *et al.* (2014) Structural insights into the function of a unique tandem GTPase EngA in bacterial ribosome assembly. *Nucleic Acids Res.*, **42**, 13430–13439.
22. Sharma,M.R., Barat,C., Wilson,D.N., Booth,T.M., Kawazoe,M., Hori-Takemoto,C., Shirouzu,M., Yokoyama,S., Fucini,P. and Agrawal,R.K. (2005) Interaction of Era with the 30S ribosomal subunit implications for 30S subunit assembly. *Mol. Cell*, **18**, 319–329.
23. Datta,P.P., Wilson,D.N., Kawazoe,M., Swami,N.K., Kaminishi,T., Sharma,M.R., Booth,T.M., Takemoto,C., Fucini,P., Yokoyama,S. *et al.* (2007) Structural aspects of RbfA action during small ribosomal subunit assembly. *Mol. Cell*, **28**, 434–445.
24. Zheng,S.Q., Palovcak,E., Armache,J.P., Verba,K.A., Cheng,Y. and Agard,D.A. (2017) MotionCor2: anisotropic correction of beam-induced motion for improved cryo-electron microscopy. *Nat. Methods*, **14**, 331–332.
25. Zhang,K. (2016) Gctf: Real-time CTF determination and correction. *J. Struct. Biol.*, **193**, 1–12.
26. Kimanius,D., Forsberg,B.O., Scheres,S.H. and Lindahl,E. (2016) Accelerated cryo-EM structure determination with parallelisation using GPUs in RELION-2. *eLife*, **5**, e18722.
27. Zivanov,J., Nakane,T., Forsberg,B.O., Kimanius,D., Hagen,W.J., Lindahl,E. and Scheres,S.H. (2018) New tools for automated high-resolution cryo-EM structure determination in RELION-3. *eLife*, **7**, e42166.
28. Scheres,S.H. (2012) RELION: implementation of a Bayesian approach to cryo-EM structure determination. *J. Struct. Biol.*, **180**, 519–530.
29. Pettersen,E.F., Goddard,T.D., Huang,C.C., Couch,G.S., Greenblatt,D.M., Meng,E.C. and Ferrin,T.E. (2004) UCSF Chimera–a visualization system for exploratory research and analysis. *J. Comput. Chem.*, **25**, 1605–1612.
30. Afonine,P.V., Poon,B.K., Read,R.J., Sobolev,O.V., Terwilliger,T.C., Urzhumtsev,A. and Adams,P.D. (2018) Real-space refinement in PHENIX for cryo-EM and crystallography. *Acta Crystallogr. D Struct Biol.*, **74**, 531–544.
31. Emsley,P. and Cowtan,K. (2004) Coot: model-building tools for molecular graphics. *Acta Crystallogr. D. Biol. Crystallogr.*, **60**, 2126–2132.
32. Emsley,P., Lohkamp,B., Scott,W.G. and Cowtan,K. (2010) Features and development of Coot. *Acta Crystallogr. D. Biol. Crystallogr.*, **66**, 486–501.

33. Terwilliger,T.C., Sobolev,O.V., Afonine,P.V. and Adams,P.D. (2018) Automated map sharpening by maximization of detail and connectivity. *Acta Crystallogr. D Struct. Biol.*, **74**, 545–559.

34. Adams,P.D., Afonine,P.V., Bunkoczi,G., Chen,V.B., Davis,I.W., Echols,N., Headd,J.J., Hung,L.W., Kapral,G.J., Grosse-Kunstleve,R.W. *et al.* (2010) PHENIX: a comprehensive Python-based system for macromolecular structure solution. *Acta Crystallogr. D. Biol. Crystallogr.*, **66**, 213–221.

35. Zhang,W., Duhr,S., Baaske,P. and Laue,E. (2014) Microscale thermophoresis for the assessment of nuclear protein-binding affinities. *Methods Mol. Biol.*, **1094**, 269–276.

36. Mueller,A.M., Breitsprecher,D., Duhr,S., Baaske,P., Schubert,T. and Langst,G. (2017) MicroScale thermophoresis: a rapid and precise method to quantify protein-nucleic acid interactions in solution. *Methods Mol. Biol.*, **1654**, 151–164.

37. Parmeggiani,A., Krab,I.M., Okamura,S., Nielsen,R.C., Nyborg,J. and Nissen,P. (2006) Structural basis of the action of pulvomycin and GE2270 A on elongation factor Tu. *Biochemistry*, **45**, 6846–6857.

38. Voorhees,R.M., Schmeing,T.M., Kelley,A.C. and Ramakrishnan,V. (2010) The mechanism for activation of GTP hydrolysis on the ribosome. *Science*, **330**, 835–838.

39. Gulati,M., Jain,N., Davis,J.H., Williamson,J.R. and Britton,R.A. (2014) Functional interaction between ribosomal protein L6 and RbgA during ribosome assembly. *PLos Genet.*, **10**, e1004694.